nature methods

BRIEF COMMUNICATION

https://doi.org/10.1038/s41592-020-0760-9

Check for updates

# Rapid mesoscale volumetric imaging of neural activity with synaptic resolution

Rongwen Lu[1,9,10], Yajie Liang[1,10], Guanghan Meng[2,10], Pengcheng Zhou[3,4,5], Karel Svoboda[1], Liam Paninski[3,4,5] and Na Ji[1,2,6,7,8] ✉

**Imaging neurons and neural circuits over large volumes at high speed and subcellular resolution is a difficult task. Incorporating a Bessel focus module into a two-photon fluorescence mesoscope, we achieved rapid volumetric imaging of neural activity over the mesoscale with synaptic resolution. We applied the technology to calcium imaging of entire dendritic spans of neurons as well as neural ensembles within multiple cortical regions over two hemispheres of the awake mouse brain.**

Neurons in the brain are highly connected. Within the neocortex, a single neuron may receive a multitude of synaptic inputs and send out projections traversing millimeters of tissue. Through these long-range connections, information flows through multiple cortical regions spanning two hemispheres. To understand computation by either a single neuron or an extended network, it is essential to monitor neural activity throughout cortical depth over large volumes, ideally at synaptic resolution. By combining a two-photon fluorescence mesoscope with a 5-mm diameter field of view (FOV)[1] and a volumetric imaging module based on Bessel focus scanning[2–5], we demonstrated rapid synapse-resolving mesoscale volumetric imaging of neural activity in the adult mouse brain in vivo.

In Bessel focus scanning, an axially extended excitation focus is scanned laterally in two dimensions to provide a projected view of the volume defined by the scanning area and the axial extent of the focus. Such a focus can be generated by illuminating the microscope objective's back focal plane with an annular pattern, with the resulting focal electric field amplitude approximating a Bessel function. Laterally confined yet axially extended, a Bessel-like focus provides synapse-resolving lateral resolution at the same volumetric imaging rate as two-dimensional (2D) scanning. We designed a compact Bessel optical module to fit between the excitation laser and the mesoscope[1], which generated a Bessel-like focus with its axial full width at half maximum (FWHM) continuously adjustable from 37 to 116 μm (Supplementary Figs. 1 and 2). Scanning the Bessel focus in 2D led to a projected view of the fluorescent structures within a volume defined by up to 20-mm$^2$ area and the axial length of the focus. For the in vivo experiments, we configured the module to generate a 0.4 numerical aperture Bessel focus with a 72-μm axial FWHM. Because focusing an annular illumination sharpens the lateral confinement of the light[6], the 0.4 numerical aperture Bessel focus had lateral FWHMs of less than 0.6 μm or about 15% higher lateral resolution than the conventional 0.6 numerical aperture ('Gaussian') focus across the entire imaging FOV (Supplementary Figs. 1 and 3). Compared to the 0.6 numerical aperture Gaussian focus, the Bessel focus elongated the axial extent of two-photon excitation by approximately 18-fold. Scanning this Bessel focus in 2D over the cortex of a Thy1-GFP line M mouse in vivo, we imaged neurites within a 4.2 mm × 4.2 mm × 100 μm volume while maintaining the ability to resolve axonal boutons (that is, varicosities along thinner and dimmer neurites[7]) and dendritic spines (that is, protrusions from thicker and brighter neurites) over the entire FOV (Fig. 1). This synapse-resolving capability was maintained even at an imaging depth of 472 μm below the dura (Supplementary Fig. 4).

Having validated the synapse-resolving capability of our microscope on the mesoscale, we next used the microscope to monitor neural activity across entire dendritic spans of cortical neurons in head-fixed awake mice. Using the remote focusing module of the mesoscope to rapidly translate the Bessel focus along the axial direction, we monitored the calcium activity of the soma and dendrites of a GCaMP6s[8]-expressing infragranular neuron (depth of soma: 586 μm) in the mouse visual cortex at high speed and synaptic resolution (Fig. 2 and Supplementary Video 1). Imaging the 301 × 450 × 612 μm volume using six 2D scans of the Bessel focus (Fig. 2b), we achieved a volumetric imaging speed of 3.2 Hz (Supplementary Video 2). In comparison, scanning the same volume with remote focusing of the Gaussian focus gave rise to a volumetric rate of 0.06 Hz (Fig. 2a), a 50-fold reduction in imaging speed and too slow for calcium imaging. The dendritic spine images by the Bessel focus were sharper than those with the Gaussian focus (Fig. 2a,b,d, insets), reflecting the increased lateral resolution of the Bessel mesoscope. In total, we detected 145 dendritic spines in this neuron. Their calcium activity profiles were dominated by transients highly synchronized with those in its dendrites and soma (Fig. 2c,d). These synchronized transients in spines and dendrites had faster temporal dynamics than those in soma. In some spines, we also detected transients independent of the synchronized events (Fig. 2d, red arrows), probably evoked by local synaptic inputs.

Two 2D scans of the Bessel focus imaged the dendrites of a L2/3 neuron within a volume of 396 × 400 × 200 μm (12–212 μm depth; Supplementary Fig. 5 and Supplementary Videos 3 and 4). Its dendritic spines exhibited both global responses synchronized with somatic firing and local isolated transients (Supplementary Fig. 5c, red arrows). We also observed local transients spanning one or a few dendritic branches (Supplementary Fig. 5c, blue arrows; Supplementary Fig. 5d, ΔF/F map; Supplementary Fig. 6), indicative

[1]Janelia Research Campus, Howard Hughes Medical Institute, Ashburn, VA, USA. [2]Department of Molecular and Cell Biology, University of California, Berkeley, CA, USA. [3]Department of Statistics, Columbia University, New York, NY, USA. [4]Department of Neuroscience, Columbia University, New York, NY, USA. [5]Zuckerman Institute, Columbia University, New York, NY, USA. [6]Department of Physics, University of California, Berkeley, CA, USA. [7]Helen Wills Neuroscience Institute, University of California, Berkeley, CA, USA. [8]Molecular Biophysics and Integrated Bioimaging Division, Lawrence Berkeley National Laboratory, Berkeley, CA, USA. [9]Present address: National Eye Institute, National Institutes of Health, Bethesda, MD, USA. [10]These authors contributed equally to this work: Rongwen Lu, Yajie Liang, Guanghan Meng. ✉e-mail: jina@berkeley.edu

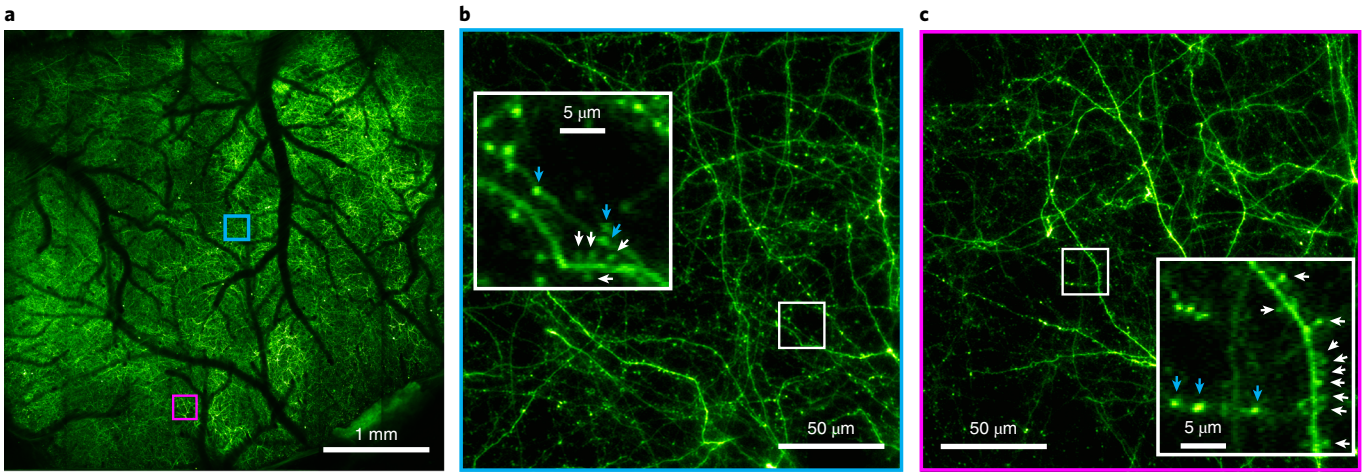


**Fig. 1 | Mesoscope volumetric imaging with synaptic resolution.** Scanning a Bessel focus in two dimensions imaged a 4.2 mm × 4.2 mm × 100 µm volume of layer 1 neurites in an awake Thy1-GFP line M mouse cortex in vivo. **a**, Entire image. **b**,**c**, Zoomed-in views. The white arrows indicate the spines; the blue arrows indicate the boutons. $n = 1$ mouse.

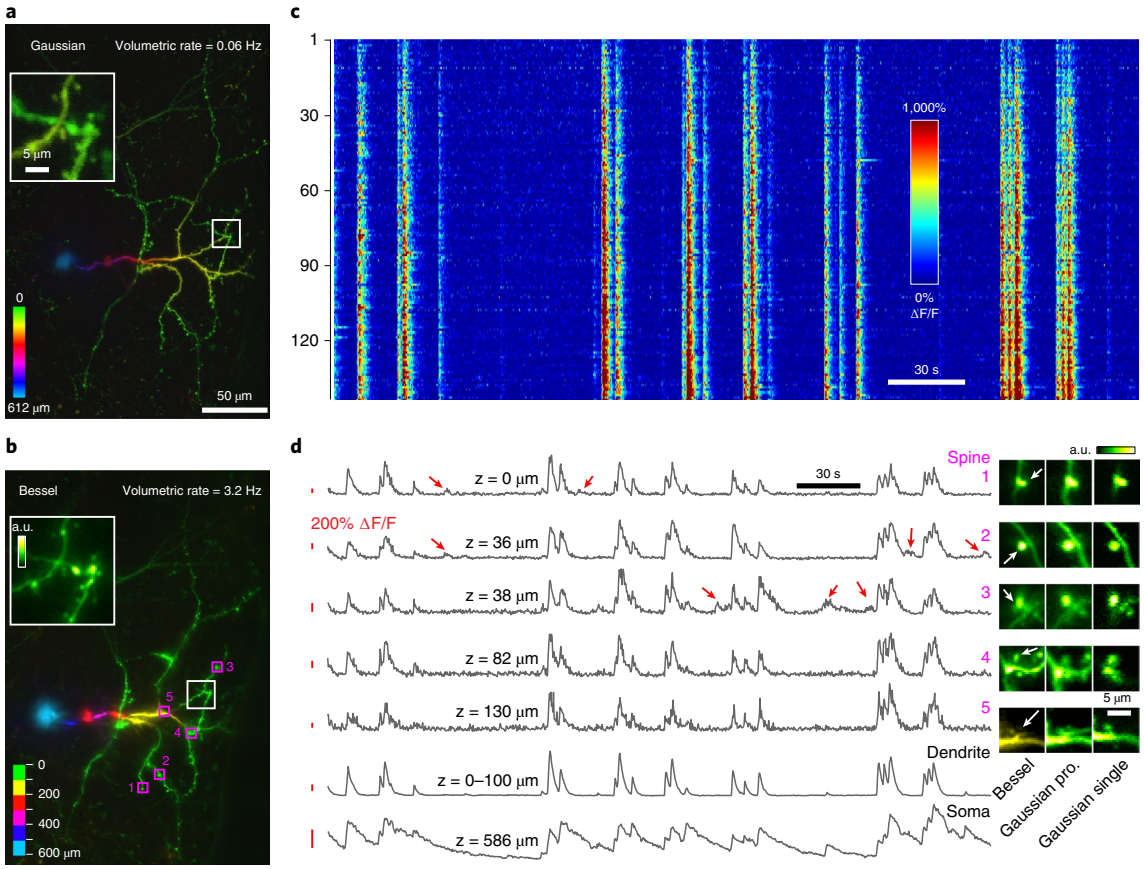


**Fig. 2 | Volumetric functional imaging across the entire dendritic spans of neurons with synaptic resolution in awake mice. a**–**d**, Recording of an infragranular neuron in a 301 × 450 × 612 µm volume. **a**, Maximum intensity projection of Gaussian image stack (307 images, 0.4-µm pixel, 2-µm z-step). **b**, Composite of six Bessel images (0.4-µm pixel, 100-µm z-step). Insets in **a** and **b**: zoomed-in views. a.u., arbitrary unit. **c**, Calcium transient ΔF/F of 145 spines. **d**, Calcium transients of example spines, dendrites and soma. The red arrows indicate local synaptic transients. Insets: images of spines in **a** (Gaussian projection), **b** (Bessel) and from a single Gaussian scan. $n = 1$ mouse. **a**, Post-objective power = 36–96 mW, increased exponentially with depth. **b**, Post-objective power = 120 mW.

of dendritic spiking[9,10]. Local synaptic transients on spines sometimes were synchronized with calcium events on distant dendritic branches and spines (Supplementary Fig 5c,d, cyan arrows), suggesting that they may share common inputs. As these two examples indicate, combining a Bessel module with fast axial scanning allows mapping the complete synaptic and dendritic activity profile of neurons, thus serving as a powerful tool in investigating neuronal computation by individual neurons. The mesoscopic FOV of our

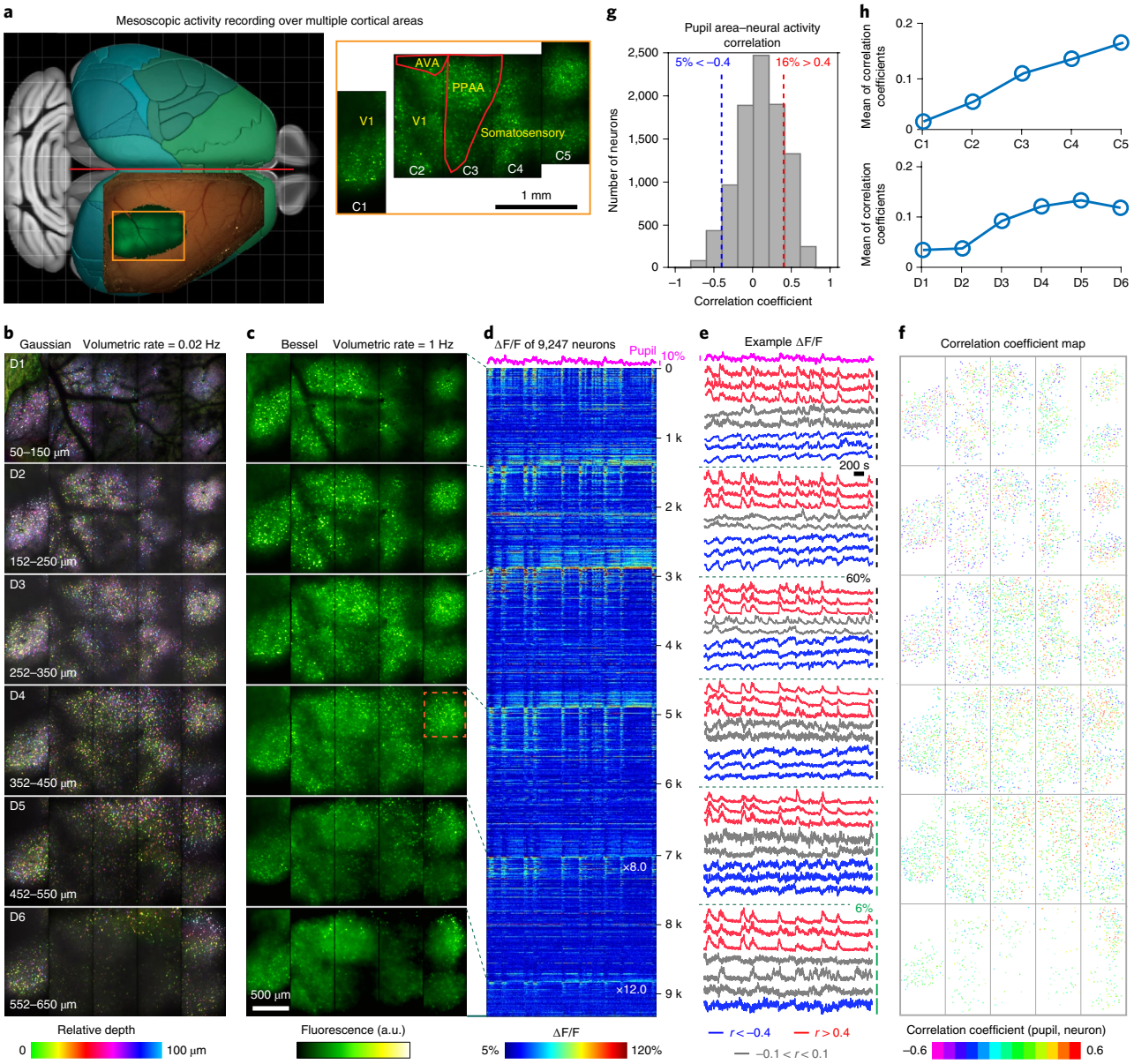


**Fig. 3 | Mesoscale volumetric functional imaging of GABAergic neuron ensembles within multiple cortical areas of an awake mouse. a**, Schematic drawing and two-photon fluorescence images showing FOV covering multiple cortical areas (C1–C5). AVA, anteromedial visual area; PPAA, posterior parietal association area; V1, primary visual cortex. **b**, Maximum intensity projections of six (D1–D6) 100-µm-thick Gaussian image stacks covering a 3,020 × 1,500 × 600 µm volume (301 images, 2-µm pixel and z-step). Post-objective power = 24–96 mW, increased exponentially with depth. **c**, Six Bessel images of the same volume (2-µm pixel, 100-µm z-step size). The orange box indicates the FOV in Supplementary Video 8. Post-objective power: 36, 51, 70, 99, 120 and 120 mW, respectively. **d**, ΔF/F of 9,247 neurons in D1–D6, sorted by decreasing correlation with pupil area (top trace). In D5 and D6, ΔF/F traces were multiplied by 8.0 and 12.0, respectively, to aid visibility. **e**, Traces of the pupil area and example calcium transients. Blue, red and gray indicate varying correlation with pupil area. **f**, Map of correlation coefficients for individual neurons. **g**, Histogram distribution of correlation coefficients. **h**, Mean of correlation coefficients of neurons in different cortical areas (top) and depths (bottom). Data were taken from $n = 1$ mouse.

system also enabled random-access volumetric imaging of neurites in distant volumes. We carried out simultaneous functional imaging of neurites in two 400 × 425 × 200 µm volumes 2 mm apart and extracted calcium traces from a total of 486 axonal boutons and dendritic spines (Supplementary Fig. 7 and Supplementary Video 5).

With the extra-large FOV, the Bessel mesoscope also enabled activity measurements of large neural ensembles over multiple cortical areas simultaneously. As an example, we studied the spontaneous activity of cortical GABAergic neurons in a head-fixed, quietly awake Gad2-IRES-Cre mouse in the dark. Previous work studying tens of inhibitory neurons within a small cortical region reported that some neurons exhibited spontaneous activity highly correlated with arousal level[4,11,12]. In the present study, we monitored spontaneous activity of GABAergic neurons spanning multiple brain areas, including the primary visual cortex (V1), the anteromedial visual area, the posterior parietal association areas and somatosensory area (Fig. 3a and Supplementary Video 6), with the mouse's pupil closely tracked and used as an indicator of arousal level. In the cortex, because GABAergic neurons are relatively sparsely distributed, within 100-µm-thick tissue we detected minimal somatic overlaps in the projected images of neurons at different depths (Fig. 3b and Supplementary Fig. 8). Therefore, scanning and then axially translating the Bessel focus six

times at 100 µm steps allowed recording the inhibitory neural activity within a volume of 3,020 × 1,500 × 600 µm (50–650 µm below the dura) at 1 Hz, a 50× gain in image rate than volumetric imaging using a Gaussian focus (Fig. 3c and Supplementary Video 7). Because subpopulations of these cytosolic GCaMP6s-expressing neurons exhibited synchronized activity, we observed highly correlated background fluctuation across the FOV. Consequently, we found that correlation-based, region of interest (ROI) segmentation algorithms[13–16] failed to accurately detect active neurons. We modified constrained nonnegative matrix factorization for microendoscopic data (CNMF-E)[16] to first segment ROIs based on local contrast of fluorescence intensity rather than local correlation and then model the neuropil background with a spatially smooth low-rank matrix (Supplementary Software and Supplementary Video 8). The optimized CNMF-E method detected 9,247 active neurons within this volume and extracted their calcium transients without background neuropil activity (Fig. 3d). Across depths and cortical areas, we observed diverse spontaneous activity patterns positively or negatively correlated with pupil area (Fig. 3e, red and blue traces for highly positive and negative correlation, respectively), as well as activity not correlated with the arousal level (Fig. 3e, gray traces). We color-coded all 9,247 neurons based on their Pearson correlation coefficients between their calcium transients and the pupil area (Fig. 3f). Within the entire neural ensemble, 16% of neurons exhibited highly correlated (correlation coefficient $r > 0.4$) and 5% highly anticorrelated ($r < -0.4$) spontaneous activity with arousal (Fig. 3g). We observed both cortical region and depth dependences in the correlation coefficient distributions of these GABAergic neurons (Supplementary Fig. 9), with the average correlation coefficients increasing from posterior to anterior and cortical depth (Fig. 3h). Similar trends were observed when the same analyses were applied to 6,613 neurons segmented by hand (Supplementary Figs. 10 and 11). Finally, with the mesoscale FOV of the microscope, we measured neural activity in three volumes of 189 L2/3 callosal projection neurons in visual cortices located in separate hemispheres at 3.1 volumes per second, 39× faster than three-dimensional (3D) scanning of Gaussian focus (Supplementary Fig. 12 and Supplementary Video 9).

In summary, by combining Bessel focus-based volumetric imaging with a mesoscope and turning the 2D frame rate into a volume rate, we achieved fast activity imaging with synaptic resolution over large mesoscale volumes. A powerful tool to interrogate the input/output transformation by individual neurons, the Bessel-module-equipped mesoscope simultaneously recorded synaptic, dendritic and somatic calcium activity of neurons spanning 600 µm in depth in a head-fixed awake mouse. Such performance is difficult for other methods to achieve[17] because of the simultaneous requirements of high spatial and temporal resolution in large volumes of opaque tissue. Unlike light sheet-based methods, which require minimal scattering of the fluorescence photons, the nonlinear excitation and the nonimaging detection of the two-photon mesoscope, where fluorescence photons were generated within a femtoliter focal volume and collected with a photomultiplier tube, enabled us to resolve synapses at depth. The axial extension of the Bessel focus also renders the resulting images resistant to axial motion artifacts, without the need for complex motion compensation[18].

At the circuit level, we took advantage of the mesoscale FOV and demonstrated simultaneous monitoring of the spontaneous activity of >9,000 GABAergic neurons within 600 µm cortical depth of four cortical areas, as well as callosal projection neurons spanning two hemispheres. Compared to conventional 3D scanning approaches, in addition to an order-of-magnitude gain in imaging speed, Bessel focusing scanning with a mesoscope also generated information-rich datasets with much smaller data sizes, facilitating image processing and data analysis.

Bessel modules can also be combined with other mesoscope systems[19,20], as well as three-photon fluorescence excitation[21–23], to further increase imaging depth. Together, they will greatly benefit system neuroscientific investigations in live brains, where activity of neural circuits underlying animal behaviors can be studied at subcellular resolution on the mesoscale across brain areas and cortical depths.

## Online content

Any methods, additional references, Nature Research reporting summaries, source data, extended data, supplementary information, acknowledgements, peer review information; details of author contributions and competing interests; and statements of data and code availability are available at https://doi.org/10.1038/s41592-020-0760-9.

Received: 16 April 2019; Accepted: 22 January 2020;
Published online: 2 March 2020

## References

1. Sofroniew, N. J., Flickinger, D., King, J. & Svoboda, K. A large field of view two-photon mesoscope with subcellular resolution for in vivo imaging. *eLife* **5**, e14472 (2016).
2. Botcherby, E. J., Juškaitis, R. & Wilson, T. Scanning two photon fluorescence microscopy with extended depth of field. *Opt. Commun.* **268**, 253–260 (2006).
3. Thériault, G., Cottet, M., Castonguay, A., McCarthy, N. & De Koninck, Y. Extended two-photon microscopy in live samples with Bessel beams: steadier focus, faster volume scans, and simpler stereoscopic imaging. *Front. Cell. Neurosci.* **8**, 139 (2014).
4. Lu, R. et al. Video-rate volumetric functional imaging of the brain at synaptic resolution. *Nat. Neurosci.* **20**, 620–628 (2017).
5. Lu, R., Tanimoto, M., Koyama, M. & Ji, N. 50 Hz volumetric functional imaging with continuously adjustable depth of focus. *Biomed. Opt. Express* **9**, 1964–1976 (2018).
6. Welford, W. T. Use of annular apertures to increase focal depth. *J. Opt. Soc. Am.* **50**, 749–752 (1960).
7. De Paola, V. et al. Cell type-specific structural plasticity of axonal branches and boutons in the adult neocortex. *Neuron* **49**, 861–875 (2006).
8. Chen, T.-W. et al. Ultrasensitive fluorescent proteins for imaging neuronal activity. *Nature* **499**, 295–300 (2013).
9. Häusser, M., Spruston, N. & Stuart, G. J. Diversity and dynamics of dendritic signaling. *Science* **290**, 739–744 (2000).
10. Manita, S., Miyakawa, H., Kitamura, K. & Murayama, M. Dendritic spikes in sensory perception. *Front. Cell. Neurosci.* **11**, 29 (2017).
11. Reimer, J. et al. Pupil fluctuations track fast switching of cortical states during quiet wakefulness. *Neuron* **84**, 355–362 (2014).
12. Pakan, J. M. et al. Behavioral-state modulation of inhibition is context-dependent and cell type specific in mouse visual cortex. *eLife* **5**, e14985 (2016).
13. Pachitariu, M. et al. Suite2p: beyond 10,000 neurons with standard two-photon microscopy. Preprint at *bioRxiv* https://www.biorxiv.org/content/10.1101/061507 (2017).
14. Liu, H., Wu, Z., Li, X., Cai, D. & Huang, T. S. Constrained nonnegative matrix factorization for image representation. *IEEE Trans. Pattern Anal. Mach. Intell.* **34**, 1299–1311 (2012).
15. Pnevmatikakis, E. A. et al. Simultaneous denoising, deconvolution, and demixing of calcium imaging data. *Neuron* **89**, 285–299 (2016).
16. Zhou, P. et al. Efficient and accurate extraction of in vivo calcium signals from microendoscopic video data. *eLife* **7**, e28728 (2018).
17. Ji, N., Freeman, J. & Smith, S. L. Technologies for imaging neural activity in large volumes. *Nat. Neurosci.* **19**, 1154–1164 (2016).
18. Szalay, G. et al. Fast 3D imaging of spine, dendritic, and neuronal assemblies in behaving animals. *Neuron* **92**, 723–738 (2016).
19. Stirman, J. N., Smith, I. T., Kudenov, M. W. & Smith, S. L. Wide field-of-view, multi-region, two-photon imaging of neuronal activity in the mammalian brain. *Nat. Biotechnol.* **34**, 857–862 (2016).
20. Tsai, P. S. et al. Ultra-large field-of-view two-photon microscopy. *Opt. Express* **23**, 13833–13847 (2015).
21. Horton, N. G. et al. *In vivo* three-photon microscopy of subcortical structures within an intact mouse brain. *Nat. Photonics* **7**, 205–209 (2013).
22. Ouzounov, D. G. et al. In vivo three-photon imaging of activity of GCaMP6-labeled neurons deep in intact mouse brain. *Nat. Methods* **14**, 388–390 (2017).
23. Rodríguez, C., Liang, Y., Lu, R. & Ji, N. Three-photon fluorescence microscopy with an axially elongated Bessel focus. *Opt. Lett.* **43**, 1914–1917 (2018).

## Methods

**Animals.** All animal experiments were conducted according to the National Institutes of Health (NIH) guidelines for animal research. Procedures and protocols used on mice were approved by the Institutional Animal Care and Use Committee at Janelia Research Campus, Howard Hughes Medical Institute. Male or female mice (C57BL/6J background) aged two months and older were used in this study and included wild-type (Black 6, stock no. 000664; The Jackson Laboratory), Gad2-IRES-Cre (*Gad2*$^{tm2(cre)Zjh}$/J, stock no. 010802; The Jackson Laboratory) and Thy1-GFP line M (Tg(Thy1-EGFP)MJrs/J, stock no. 007788; The Jackson Laboratory) strains. Mice were housed in cages in groups of 1–5 before surgery under a reverse light cycle.

**Stereotaxic surgery for in vivo imaging.** All surgeries were performed using a stereotaxic apparatus (Model 1900, David Kopf Instruments) and aseptic technique, as described previously[1,4]. Briefly, mice were anesthetized with isoflurane (1–2% by volume in $O_2$) and given the analgesic buprenorphine (subcutaneously, 0.3 mg per kg of body weight). A craniotomy was made over one dorsal hemisphere or across the two hemispheres with the dura left intact. For mice that required virus injection, a glass pipette (Drummond Scientific) beveled at 45° with a 15–20-µm opening was back-filled with mineral oil. A fitted plunger controlled by a hydraulic manipulator (MO10; Narishige) was inserted into the pipette and used to load and slowly inject 10–20 nl viral solution into the brain at approximately 200–400 µm below the pia mater. The following injection coordinates (in mm) were chosen to label brain regions in one or both hemispheres: site 1 (bregma: −4.6; midline: 2.1); site 2 (bregma: −4.6; midline: 2.8); site 3 (bregma: −4.1; midline: 2.1); site 4 (bregma: −4.1; midline: 2.8); site 5 (bregma: −3.5; midline: 2.1); site 6 (bregma: −3.5; midline: 2.8); site 7 (bregma: −3.0; midline: 2.1); site 8 (bregma: −3.0; midline: 2.8).

For sparse labeling of neurons in 1 hemisphere, AAV2/1.syn.FLEX.GCaMP6s ($1\times10^{13}$ genome copies per ml) was mixed with AAV2/1.syn.Cre ($1\times10^{13}$ genome copies per ml diluted 10,000 times) at 1:1 for injection into wild-type mice. To label GABAergic neurons, AAV2/1.syn.FLEX.GCaMP6s ($1\times10^{13}$ genome copies per ml) was injected into Gad2-IRES-Cre mice. To label the callosal projection neurons in both hemispheres, AAV2/1.syn.FLEX.GCaMP6s ($1\times10^{13}$ genome copies per ml) was mixed with retroAAV.CAG.FlipO ($2\times10^{12}$ genome copies per ml) at 1:1 for injection into the left hemisphere at the aforementioned coordinates, and AAV2/1.CAG.FRT.GCaMP6s ($3.9\times10^{12}$ genome copies ml) was mixed with retroAAV.syn.Cre ($1\times10^{13}$ genome copies per ml) at 1:1 for injection into the right hemisphere at the aforementioned coordinates in wild-type mice. At completion of the viral injections or craniotomy without viral injections, a 450-µm-thick custom-made glass window fitting the shape of the craniotomy was embedded and sealed in place with dental acrylic. A titanium headpost was then attached to the skull with cyanoacrylate glue and dental acrylic. In vivo imaging was carried out after at least two weeks of recovery with single or paired housing and habituation for head fixation. All imaging experiments were carried out on head-fixed awake mice.

**Two-photon fluorescence mesoscope with a Bessel module.** The two-photon fluorescence mesoscope (Supplementary Fig. 1a) was described in detail previously[1]. In its conventional operation mode ('Gaussian mode'), after beam expansion, the excitation laser first entered the remote focusing unit and was focused by an objective onto a mirror mounted on a voice coil. A polarized beam splitter and a quarter-wave plate directed the back-reflected light toward the scanning optics. Pupil relay PR1 imaged the back focal plane of the remote focusing objective onto a resonant scanner that scanned the focus along the *x* axis at a 24 kHz line rate. After pupil relay PR-2, the excitation light was scanned by a virtually conjugated Galvo pair, consisting of two X-Galvo mirrors and one Y-Galvo mirror. The two X-Galvo mirrors scanned synchronously to keep the beam stationary at the Y-Galvo mirror without needing a pupil relay made of refractive optics. Directing the excitation laser to different locations in the FOV, the virtually conjugated Galvo pair unit enabled the transition time between two imaging areas to within 3.4 ms. Finally, the Y-Galvo was optically conjugated by the pupil relay PR3 to the back focal plane of the imaging objective of an illumination numerical aperture of 0.6 and collection numerical aperture of 1.0.

Using the optical prescriptions of the mesoscope, we designed an axicon-based compact Bessel module following the principles detailed previously[5]. The module was composed of an axicon, three lenses (L1, L2 and L3) and an annular mask, and was fitted between the excitation laser and the scanning optics of a mesoscope (Supplementary Fig. 1a). The module was mounted on a 12×12″ breadboard and attached to the mesoscope using two angle brackets (Supplementary Fig. 1 and Supplementary data). The module contained two mirrors mounted on a motorized stage. When inserted into the path of the excitation laser, mirror M1 directed the light into the Bessel module; after it propagated through the module, mirror M2 directed the excitation light back into the mesoscope. Together, they enabled us to conveniently and reproducibly switch between the Bessel and Gaussian focus scanning modalities without requiring realignment of the optical path. In the Bessel module, after the excitation laser was directed to propagate through the axicon (that is, a conical lens), it formed an annular illumination at the focal plane of lens L1 (focal length: 125 mm), where an annular mask was placed to spatially filter the annular illumination to achieve a desired axial intensity profile. The lens pair L2 and L3 then relayed the filtered annular illumination onto the back focal plane of the remote focusing objective and eventually the back focal plane of the imaging objective via PR1, PR2 and PR3 (Supplementary Fig. 1a). To avoid changing the optical layout of the mesoscope, lens L3 had to be at least 330 mm away from the back focal plane of the remote focusing objective. To make the module compact, we chose L2 and L3 to have relatively short focal lengths (L2, 75 mm; L3, 250 mm). To maintain optical conjugation between the mask and the remote focusing objective back focal plane, instead of the usual 4f configuration for L2 and L3, we used the following distances: annular mask to L2: $75-(330-250)/(330/75)^2$ mm = 70.8 mm; L2 to L3: 325 mm; L3 to remote focusing back focal plane: 330 mm. See Supplementary Note 1 for assembly and alignment of the Bessel module. The radius and thickness of the annulus determined the lateral resolution and axial extent of the focus, respectively[4]. To adjust the axial length of the Bessel beam focus, we either displaced L2 along the direction of beam propagation[5] or varied the beam size on the axicon[24] (Supplementary Fig. 2). We measured the excitation point spread functions across the mesoscope FOV for both Gaussian and Bessel configurations (Supplementary Fig. 3) with 0.2-µm-diameter fluorescent beads.

**Automatic detection of ROIs and extraction of calcium transients from mesoscopic volumetric activity data.** All in vivo images were registered in two dimensions with either a piecewise[25] or full-frame iterative cross-correlation-based rigid motion correction algorithm[26]. Because neuron shapes in this study were consistently quasi-ellipsoidal and neurons were not densely packed, we could use a template-matching method to detect cell locations and create ROI masks for individual neurons. However, the activity of neurons cannot be simply extracted by averaging pixels within each ROI because the background fluctuations were highly correlated with the neural signal (with some correlation coefficients >0.7) and individual neuronal signals were also highly correlated. We developed a simple solution to separate the signals of individual neurons from the background, based on the empirical observation that the background is spatially smoother than the shape of a single neuron; see Zhou et al.[16] for a related approach.

We began by estimating the background values of the pixels outside the ROIs of all neurons using a low-rank matrix factorization model, and then filled the background values with the ROIs of neurons by interpolating the pixel values on the ROI boundaries. The low-rank approximation ensures that the background sources have large spatial ranges and the interpolating strategy preserves the spatial smoothness of these sources. Once the background is estimated, extracting the shape and activity of a single neuron can be simply done by running a rank-1 matrix factorization on the background-subtracted data within each ROI. (See Supplementary Note 2 for details of the algorithm.)

For the most part, the extracted ΔF/F did not include surrounding neuropil activity due to the background subtraction described earlier. However, signal contamination by out-of-focus excitation of fluorescence structures near the cortical surface constituted a time-invariant additional background signal, which was absorbed into the baselines (*F*) of detected ROIs and remained throughout the processing pipeline. Since this out-of-focus background fluorescence increased exponentially with imaging depth, neurons at a 450–650 µm depth had artifactually small ΔF/F values (Fig. 3c,d), which nevertheless did not affect the correlation computation, or the conclusions related to the data shown in Fig. 3.

To validate the automatic neuropil subtraction approach employed in the present study, we compared these calcium transients with those obtained with the more established method of neuropil subtraction ('surrounding pixel neuropil subtraction'), where the fluorescence signal from pixels surrounding each ROI was used to calculate the neuropil contribution[4,8,27]. The calcium transients calculated for the same neuron showed high correlation coefficient across all depths (Supplementary Fig. 13 and Supplementary Video 10), indicating that our CNMF-E pipeline produced very similar traces to those from the standard method of neuropil subtraction. A closer look at the 2% of neurons with correlation coefficients <0.6 indicates that they fell within three categories: (1) neurons whose neuropil mask contained nearby cell bodies, causing errors to the surrounding pixel subtraction method; (2) neurons close to image borders with fewer surrounding pixels for background estimation; and (3) neurons with very noisy activity traces. For both (1) and (2), the CNMF-E pipeline should provide more accurate estimation since it does not rely exclusively on the local pixels. For case (3), these neurons do not generally provide useful information; thus, they can be ignored in the final analysis.

**Additional data processing.** For manually segmented ROIs representing neuronal cell bodies (Supplementary Figs. 10 and 12), neuropil background contamination was removed from the signal using surrounding pixel neuropil subtraction. Because this approach is only accurate when the pixels surrounding the ROIs are not over other cell bodies, we excluded neurons with contiguous neighboring cells from our analysis.

The ΔF/F traces in Supplementary Fig. 5c were smoothed by a Gaussian filter with size = 3 and s.d. = 2. A Gaussian filter with size = 5 and s.d. = 3 was used to smooth the ΔF/F traces extracted from both automatically (Fig. 3) and manually (Supplementary Figs. 10 and 12) segmented ROIs, as well as the trace of the pupil area. Correlation coefficients were calculated using the smoothed traces.

**Upper bound for labeling density for volumetric imaging using Bessel focus scanning.** To unambiguously detect and identify an active structure (bouton, spine or soma) in a Bessel imaging time series, during the response duration $T$ of the activity indicator, there should only be a single active structure within the volume $A \times L$, where $A$ is the area of the structure in the lateral plane and $L$ is the axial length of the Bessel focus. Given $\rho$ as the volume density of labeled structures, and an activity rate of $P$ (number of activity events per second), the aforementioned requirement translates into $A \times L \times \rho \times P \times T \leq 1$. This leads to an upper bound on the labeling density:

$$\rho \leq 1/(A \times L \times T \times P)$$

This upper bound is inversely proportional to the area of the structure, the length of the Bessel focus, the response time of the sensor and the frequency of active events. In other words, smaller structures, shorter Bessel beam, faster sensors and lower firing probability allow higher densities of neuronal structures to be studied with the Bessel focus scanning method. (In the present study, we assume that the $\Delta F$ due to a single active structure can be detected above the baseline fluorescence $F$ from multiple labeled structures at different depths, for which activity sensors with high contrast and low basal fluorescence are advantageous.).

We can estimate the upper bound for the following hypothetical condition. Given a cell body area $A$ of 100 $\mu m^2$, a Bessel focus that probes a 100 µm depth range, $T$ being 2 s for GCaMP6s and $P$ being 2 action potentials per second, the maximum $\rho$ is 25,000 cell bodies per $mm^3$. In comparison, the density of the GCaMP6s$^+$ GABAergic neurons in Fig. 3 is 3,402 neurons per $mm^3$.

**Reporting Summary.** Further information on research design is available in the Nature Research Reporting Summary linked to this article.

## Data availability

The raw calcium imaging data for Figs. 2 and 3 are available at https://doi.org/10.6084/m9.figshare.11639787 and https://doi.org/10.6084/m9.figshare.11629098.v4.

## Code availability

The custom CNMF-E processing codes in MATLAB are included as Supplementary Software.

## References

24. Thériault, G., De Koninck, Y. & McCarthy, N. Extended depth of field microscopy for rapid volumetric two-photon imaging. *Opt. Express* **21**, 10095–10104 (2013).
25. Pnevmatikakis, E. A. & Giovannucci, A. NoRMCorre: an online algorithm for piecewise rigid motion correction of calcium imaging data. *J. Neurosci. Methods* **291**, 83–94 (2017).
26. Guizar-Sicairos, M., Thurman, S. T. & Fienup, J. R. Efficient subpixel image registration algorithms. *Opt. Lett.* **33**, 156–158 (2008).
27. Kerlin, A. M., Andermann, M. L., Berezovskii, V. K. & Reid, R. C. Broadly tuned response properties of diverse inhibitory neuron subtypes in mouse visual cortex. *Neuron* **67**, 858–871 (2010).

## Acknowledgements

The authors thank N. Sofroniew for demonstrations on cranial window preparation; D. Flickinger for troubleshooting, optical alignments and helpful discussions; B. Mohar and A. Kerlin for help with system alignments and ScanImage operations; V. Custard for administrative support; J. Zheng for assistance with ScanImage; and M. Pachitariu for sharing the mesoscope and helpful discussions. R.L., Y.L., K.S. and N.J. were supported by the Howard Hughes Medical Institute. G.M. and N.J. were supported by NIH grant no. NINDS U01NS103489. P.Z. and L.P. were supported by NIH grant nos. R01-EB22913 and U01NS103489, the National Science Foundation (NeuroNex award no. DBI-1707398) and the Gatsby Foundation (GAT3708).

## Author contributions

N.J. conceived and supervised the project. R.L., Y.L., K.S. and N.J. designed the experiments. R.L. designed and built the Bessel module. Y.L. performed the mouse surgery. R.L. and Y.L. collected the data. P.Z. and L.P. developed the automatic ROI detection codes. R.L. and G.M. analyzed the data. All authors contributed to the preparation of the manuscript.

## Competing interests

The mesoscope (K.S.) and Bessel focus scanning (R.L. and N.J.) intellectual property has been licensed to Thorlabs by the Howard Hughes Medical Institute.

## Additional information

**Supplementary information** is available for this paper at https://doi.org/10.1038/s41592-020-0760-9.

**Correspondence and requests for materials** should be addressed to N.J.

**Peer review information** Nina Vogt was the primary editor on this article and managed its editorial process and peer review in collaboration with the rest of the editorial team.

**Reprints and permissions information** is available at www.nature.com/reprints.

nature research

Corresponding author(s): Na Ji

Last updated by author(s): Nov 10, 2019

# Reporting Summary

Nature Research wishes to improve the reproducibility of the work that we publish. This form provides structure for consistency and transparency in reporting. For further information on Nature Research policies, see Authors & Referees and the Editorial Policy Checklist.

## Statistics

For all statistical analyses, confirm that the following items are present in the figure legend, table legend, main text, or Methods section.

| n/a | Confirmed | |
|---|---|---|
| ☐ | ☒ | The exact sample size (*n*) for each experimental group/condition, given as a discrete number and unit of measurement |
| ☐ | ☒ | A statement on whether measurements were taken from distinct samples or whether the same sample was measured repeatedly |
| ☐ | ☒ | The statistical test(s) used AND whether they are one- or two-sided<br>*Only common tests should be described solely by name; describe more complex techniques in the Methods section.* |
| ☒ | ☐ | A description of all covariates tested |
| ☒ | ☐ | A description of any assumptions or corrections, such as tests of normality and adjustment for multiple comparisons |
| ☒ | ☐ | A full description of the statistical parameters including central tendency (e.g. means) or other basic estimates (e.g. regression coefficient) AND variation (e.g. standard deviation) or associated estimates of uncertainty (e.g. confidence intervals) |
| ☒ | ☐ | For null hypothesis testing, the test statistic (e.g. *F*, *t*, *r*) with confidence intervals, effect sizes, degrees of freedom and *P* value noted<br>*Give P values as exact values whenever suitable.* |
| ☒ | ☐ | For Bayesian analysis, information on the choice of priors and Markov chain Monte Carlo settings |
| ☒ | ☐ | For hierarchical and complex designs, identification of the appropriate level for tests and full reporting of outcomes |
| ☐ | ☒ | Estimates of effect sizes (e.g. Cohen's *d*, Pearson's *r*), indicating how they were calculated |

*Our web collection on statistics for biologists contains articles on many of the points above.*

## Software and code

Policy information about availability of computer code

| | |
|---|---|
| Data collection | ScanImage 2015b (http://scanimage.vidriotechnologies.com/display/SIH/ScanImage+Home) was used for data collection. |
| Data analysis | MATLAB 2017 and above, CNMF-E package, FIJI-Win64 were used for data processing. |

For manuscripts utilizing custom algorithms or software that are central to the research but not yet described in published literature, software must be made available to editors/reviewers. We strongly encourage code deposition in a community repository (e.g. GitHub). See the Nature Research guidelines for submitting code & software for further information.

## Data

Policy information about availability of data

All manuscripts must include a data availability statement. This statement should provide the following information, where applicable:

- Accession codes, unique identifiers, or web links for publicly available datasets
- A list of figures that have associated raw data
- A description of any restrictions on data availability

The data that support the findings of this study are available from the corresponding author upon reasonable request.

# Field-specific reporting

Please select the one below that is the best fit for your research. If you are not sure, read the appropriate sections before making your selection.

☒ Life sciences ☐ Behavioural & social sciences ☐ Ecological, evolutionary & environmental sciences

For a reference copy of the document with all sections, see nature.com/documents/nr-reporting-summary-flat.pdf

# Life sciences study design

All studies must disclose on these points even when the disclosure is negative.

| | |
|---|---|
| Sample size | The purpose of this manuscript is to develop a new rapid mesoscale two-photon volumetric imaging method for recording neuronal activity with synaptic resolution in the mouse brain. In total 4 mice were used to demonstrate imaging performance in the manuscript. First, we used a Thy-1 GFP line M mouse to demonstrate the synaptic resolution and mesoscale field of view (4.2 mm x 4.2 mm). Next, we used another mouse for the demonstration of volumetric functional imaging of entire dendritic spans. After that, we used one mouse to demonstrate mesocale volumetric functional imaging of neuronal ensembles over four cortical areas of the same hemisphere. Last, we used the 4th mouse to demonstrate mesoscale volumetric functional imaging of callosal-projection neurons across two hemispheres of an awake mouse. |
| Data exclusions | NONE |
| Replication | Four mice were used for the study. As the manuscript is focused on demonstrating the capability of a microscopy technique, rather than reaching biological conclusions, we did not extensively replicate the experiments. |
| Randomization | Animals in the colony were chosen randomly for the study. As the manuscript is focused on demonstrating the capability of a microscopy technique, rather than reaching biological conclusions, randomization does not apply to this study. |
| Blinding | No blinding was required here. Three lines of mice were used: C57BL/6J, GAD2-IRES-cre, and TYP1-GFP line M. They underwent similar surgery, recovery and imaging protocols. For our imaging experiments, it became obvious once we start imaging the brain whether the mice have fluorescence expression. Therefore, no blinding was used. |

# Reporting for specific materials, systems and methods

We require information from authors about some types of materials, experimental systems and methods used in many studies. Here, indicate whether each material, system or method listed is relevant to your study. If you are not sure if a list item applies to your research, read the appropriate section before selecting a response.

## Materials & experimental systems

| n/a | Involved in the study |
|---|---|
| ☒ | ☐ Antibodies |
| ☒ | ☐ Eukaryotic cell lines |
| ☒ | ☐ Palaeontology |
| ☐ | ☒ Animals and other organisms |
| ☒ | ☐ Human research participants |
| ☒ | ☐ Clinical data |

## Methods

| n/a | Involved in the study |
|---|---|
| ☒ | ☐ ChIP-seq |
| ☒ | ☐ Flow cytometry |
| ☒ | ☐ MRI-based neuroimaging |

## Animals and other organisms

Policy information about studies involving animals; ARRIVE guidelines recommended for reporting animal research

| | |
|---|---|
| Laboratory animals | Male or female mice (C57BL/6J background) aged two months and older were used in this study and included wild-type (Jackson Laboratories, Black 6, stock #:000664), Gad2-IRES-cre (Jackson Laboratories, Gad2tm2(cre)Zjh/J, stock #: 010802), and Thy1-GFP line M (Jackson Laboratories, Tg(Thy1-EGFP)MJrs/J, stock #: 007788) strains. Mice were housed in cages in groups of 1–5 before surgeries under reverse light cycle. |
| Wild animals | The study did not involve wild animals. |
| Field-collected samples | The study did not involve field-collected samples. |
| Ethics oversight | All animal experiments were conducted according to the National Institutes of Health guidelines for animal research. Procedures and protocols on mice were approved by the Institutional Animal Care and Use Committee at Janelia Research Campus, Howard Hughes Medical Institute. |

Note that full information on the approval of the study protocol must also be provided in the manuscript.